

Vacuum-field-induced state mixing

Diego Fernández de la Pradilla^{1*}, Esteban Moreno¹ and Johannes Feist¹

¹ Departamento de Física Teórica de la Materia Condensada and Condensed Matter Physics Center (IFIMAC), Universidad Autónoma de Madrid, E-28049 Madrid, Spain

* diego.fernandez@uam.es

October 7, 2023

1 Abstract

2 By engineering the electromagnetic vacuum field, the induced Casimir-Polder shift (also
3 known as Lamb shift) and spontaneous emission rates of individual atomic levels can
4 be controlled. When the strength of these effects becomes comparable to the energy
5 difference between two previously uncoupled atomic states, an environment-induced
6 interaction between these states appears after tracing over the environment. This inter-
7 action has been previously studied for degenerate levels and simple geometries involving
8 infinite, perfectly conducting half-spaces or free space. Here, we generalize these studies
9 by developing a convenient description that permits the analysis of these non-diagonal
10 perturbations to the atomic Hamiltonian in terms of an accurate non-Hermitian Hamil-
11 tonian. Applying this theory to a hydrogen atom close to a dielectric nanoparticle, we
12 show strong vacuum-field-induced state mixing that leads to drastic modifications in both
13 the energies and decay rates compared to conventional diagonal perturbation theory. In
14 particular, contrary to the expected Purcell enhancement, we find a surprising decrease of
15 decay rates within a considerable range of atom-nanoparticle separations. Furthermore,
16 we quantify the large degree of mixing of the unperturbed eigenstates due to the non-
17 diagonal perturbation. Our work opens new quantum state manipulation possibilities in
18 emitters with closely spaced energy levels.

19

20 Contents

21	1 Introduction	2
22	2 Methods	3
23	2.1 Macroscopic quantum electrodynamics	3
24	2.2 Master equation and effective non-Hermitian Hamiltonian	4
25	3 Results	6
26	4 Conclusion	8
27	A Derivation of the master equation	9
28	A.1 Comments on the Bloch-Redfield master equation	9
29	A.2 Lindblad master equation with full secularization	9
30	A.3 Lindblad master equation: derivation details and proof	10
31	B Derivation of the effective Hamiltonian	12
32	B.1 Angular momentum conservation	13

33	C Numerical check	13
34	References	15

35
36

37 1 Introduction

38 It is well known that atomic properties are modified due to the interaction with the quantized
39 electromagnetic (EM) vacuum field supported by macroscopic bodies [1]. In the weak-coupling
40 regime, this changes both the atomic linewidths (Purcell effect) [2] and energies (Lamb or
41 Casimir-Polder [CP] shifts) [3]. These modifications have wide-ranging applications in fields
42 such as optics or atomic and soft matter physics, including the design of efficient single photon
43 sources [4–6], the atomic force microscope [7], new atom trapping methods [8,9] or the precise
44 manipulation of atomic properties with tunable nanostructures [10]. Theoretical descriptions
45 of these effects are commonly perturbative, using either standard perturbation theory or open
46 quantum systems approaches [11], although efforts to go beyond the purely perturbative
47 regime have also been published [12–14]. When the interactions are weak, the effect of
48 the environment is customarily treated for each atomic state independently, giving rise to
49 simple diagonal energy shifts and decay rates. However, for subsets of near-degenerate atomic
50 states, the CP shift and/or spontaneous emission rates may be of the same order as the energy
51 differences within the subset, suggesting that the above treatment is not consistent, even if the
52 light-matter coupling is perturbative. This has been discussed in the literature for atoms in free
53 space [15,16].

54 In this work, we show that the standard diagonal perturbation approach indeed fails when
55 field-induced shifts are comparable to the energy level differences, requiring the treatment
56 of environment-induced interactions between the levels [17,18]. Recently, this issue has
57 been tackled with an open quantum systems’ framework designed for structures with closely
58 spaced levels [19]. In that work, the standard Bloch-Redfield equation [11] was turned into a
59 Lindblad equation [20], with the corresponding benefit of guaranteed positive populations,
60 while simultaneously eluding the usual secular approximation that neglects the couplings
61 between non-degenerate states [21]. Here, we extend this framework to incorporate the effect
62 of the counter-rotating terms in the light-matter Hamiltonian and construct a master equation
63 that accurately represents the off-diagonal CP and decay terms, which we expect to be relevant
64 in any system with subsets of near-degenerate levels. From the Lindblad equation, we extract
65 an effective non-Hermitian Hamiltonian that determines the dynamics of a subset of levels
66 and in turn enables a quantitative exploration of the vacuum-field-induced state mixing. We
67 illustrate the effects of the off-diagonal terms by applying the above steps to a system comprised
68 of a hydrogen atom close to an aluminum nitride (AlN) nanoparticle (NP), and study the impact
69 of the off-diagonal couplings on the dynamics of the atom. We find strong modifications to
70 the level structure and observe significant state mixing at atom-NP separations on the order
71 of 100 nm. Consequently, the atomic dynamics close to the NP cannot be understood without
72 consideration of the effects discussed in this work. The situation treated here lies between
73 conventional weak coupling (where light-matter interactions can be treated perturbatively
74 and states can be considered independently) and strong coupling (where light and matter
75 excitations mix significantly due to non-perturbative interactions). In this novel regime of
76 “strong weak coupling”, perturbative light-matter interactions lead to significant state mixing
77 within the matter component.

78 2 Methods

79 2.1 Macroscopic quantum electrodynamics

80 We describe the interaction between atoms and the EM field supported by macroscopic bodies
81 within macroscopic quantum electrodynamics (MQED) [22–24]. The corresponding Power-
82 Zienau-Woolley light-matter Hamiltonian in the dipole approximation [3, 25–27] is

$$H = H_{\text{at}} + H_f - \mathbf{d} \cdot \mathbf{E}(\mathbf{r}_{\text{at}}). \quad (1)$$

83 Here, H_{at} is the matter Hamiltonian, emphasizing that we treat a single atom. The field
84 Hamiltonian,

$$H_f = \sum_{\lambda} \int d^3r \int d\omega \hbar\omega \mathbf{f}_{\lambda}^{\dagger}(\mathbf{r}, \omega) \cdot \mathbf{f}_{\lambda}(\mathbf{r}, \omega), \quad (2)$$

85 contains the (bosonic) polaritonic annihilation and creation operators $\mathbf{f}_{\lambda}(\mathbf{r}, \omega)$ and $\mathbf{f}_{\lambda}^{\dagger}(\mathbf{r}, \omega)$ that
86 describe both the purely electromagnetic and the macroscopic polarization fields. Here, the
87 index $\lambda = \{e, m\}$ labels the electric or magnetic nature of the excitations, and the integrals are
88 over all space and over all positive frequencies. The last term is the dipolar interaction between
89 the atom with dipole operator \mathbf{d} and the electric field $\mathbf{E}(\mathbf{r})$ evaluated at the atomic position \mathbf{r}_{at} ,
90 where

$$\mathbf{E}(\mathbf{r}) = \sum_{\lambda} \int d^3s \int d\omega \mathbf{G}_{\lambda}(\mathbf{r}, \mathbf{s}, \omega) \cdot \mathbf{f}_{\lambda}(\mathbf{s}, \omega) + \text{H.c.}, \quad (3)$$

91 with

$$\begin{aligned} \mathbf{G}_e(\mathbf{r}, \mathbf{s}, \omega) &= i \frac{\omega^2}{c^2} \sqrt{\frac{\hbar}{\pi \epsilon_0} \text{Im} \epsilon(\mathbf{s}, \omega)} \mathbf{G}(\mathbf{r}, \mathbf{s}, \omega), \\ \mathbf{G}_m(\mathbf{r}, \mathbf{s}, \omega) &= i \frac{\omega}{c} \sqrt{\frac{\hbar}{\pi \epsilon_0} \frac{\text{Im} \mu(\mathbf{s}, \omega)}{|\mu(\mathbf{s}, \omega)|^2}} \left[\nabla_{\mathbf{s}} \times \mathbf{G}(\mathbf{s}, \mathbf{r}, \omega) \right]^T. \end{aligned}$$

92 Here, ϵ and μ stand for the electric and magnetic response functions, respectively. $\mathbf{G} =$
93 $\mathbf{G}^0 + \mathbf{G}^{\text{scatt}}$ is the classical electromagnetic Green tensor, separated in its free-space and scattering
94 contributions. In the weak-coupling regime, \mathbf{G}^0 is responsible for the free-space Lamb shift [3],
95 a NP-independent contribution that can be simply reabsorbed in H_{at} . Compared to the effects
96 we study in this work, this is a negligible correction that we discard entirely in the following.

97 For concreteness, we focus on a hydrogen atom interacting with a spheroidal AlN NP (see
98 [Figure 1a](#)). It should be noted, however, that the following arguments are of broader generality
99 and applicable to a wide range of physical systems, provided that the energies and transition
100 dipole moments of the atom and the Green tensor of the nanostructure are accessible, a general
101 requirement of CP calculations. We choose this NP shape and material for two reasons: (i) the
102 EM resonances along the symmetry axis (z) enhance the atomic transitions mediated by E_z with
103 respect to the other components, and (ii) the energy range of the EM resonances coincides with
104 the hydrogenic transition we want to target. Hence, this system provides a realistic and not
105 overly complicated testing ground for the formalism developed, and will allow us to illustrate
106 the effects of the off-diagonal vacuum shifts.

107 In [Equation 1](#), H_{at} is diagonal, and its eigenvalues include fine structure corrections [28]:

$$E_{nj} = \left(-\frac{1}{2n^2} - \frac{\alpha^2}{2n^3} \left[\frac{1}{j + \frac{1}{2}} - \frac{3}{4n} \right] \right) E_h, \quad (4)$$

108 where n , j , α and $E_h \simeq 27.2$ eV are the main quantum number, the total electronic angular
109 momentum, the fine structure constant and the Hartree energy, respectively. The energy levels,

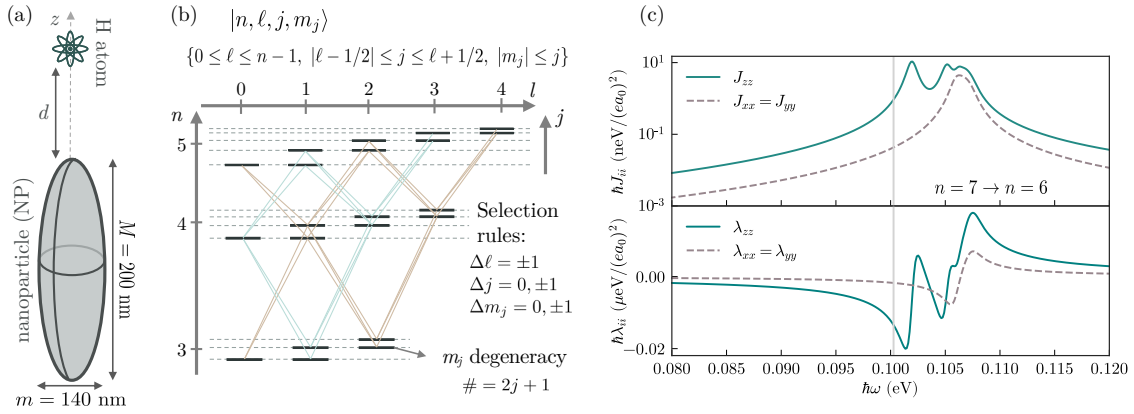


Figure 1: (a) Sketch of the system. (b) Simplified level structure of the hydrogen atom with Bohr levels and fine structure splitting (not to scale). Diagonal lines: dipolar transitions allowed from the $n = 4$ Bohr level to the $n = 5$ and $n = 3$ Bohr levels. (c) Top: spectral density of the AlN NP, obtained by setting $d = 50$ nm in Equation 7, bottom: result of the integral in Equation 6d. e is the absolute value of the charge of the electron and a_0 is the Bohr radius. Vertical line: transition frequencies of the atom from $n = 7$ to $n = 6$.

110 schematically shown in Figure 1b, are distributed in well-separated Bohr levels labeled by n ,
 111 corrected with the fine structure splitting Δ_F , a j -dependent quantity that is 4 or more orders of
 112 magnitude smaller. This energy scale is small enough that the CP induced interaction between
 113 fine structure states with the same n can be relevant. The NP is a spheroid with major and
 114 minor axes $M = 200$ nm and $m = 140$ nm, with the AlN dielectric permittivity taken from [29].
 115 For this NP, the phonon-polariton resonances lie close to the transition energy between the
 116 hydrogenic $n = 7$ and $n = 6$ states. Specifically, we will focus on the off-diagonal effects within
 117 the $n = 7$ level for an atom located along the symmetry axis z of the NP.

118 2.2 Master equation and effective non-Hermitian Hamiltonian

119 To describe the dynamics of the field-modified atomic levels and their mixing, we derive a Lind-
 120 blad equation for the atomic density matrix ρ by considering the EM fields as a weakly coupled
 121 bath and perturbatively tracing out the EM degrees of freedom. We start from the standard
 122 open quantum systems approach, which leads to the so-called Bloch-Redfield equation [11, 30]:

$$\begin{aligned}
 \dot{\rho} = & -\frac{i}{\hbar} [H_{\text{at}}, \rho] + \sum_{abcd} \left[-i(\Lambda_{ca,db}(\omega_{bd})|a\rangle\langle c|d\rangle\langle b|\rho - \Lambda_{ca,db}(\omega_{ac})\rho|a\rangle\langle c|d\rangle\langle b|) \right. \\
 & + i[\Lambda_{ca,db}(\omega_{bd}) - \Lambda_{ca,db}(\omega_{ac})]|d\rangle\langle b|\rho|a\rangle\langle c| \\
 & - \frac{1}{2}(\Gamma_{ca,db}(\omega_{bd})|a\rangle\langle c|d\rangle\langle b|\rho + \Gamma_{ca,db}(\omega_{ac})\rho|a\rangle\langle c|d\rangle\langle b|) \\
 & \left. + \frac{1}{2}[\Gamma_{ca,db}(\omega_{bd}) + \Gamma_{ca,db}(\omega_{ac})]|d\rangle\langle b|\rho|a\rangle\langle c| \right], \quad (5)
 \end{aligned}$$

123 where ρ is the atomic density matrix, the Latin indices a, b, c, d denote atomic eigenstates and
 124 $\omega_{ab} = (E_a - E_b)/\hbar$. The rotationally invariant quantities $\Gamma_{ca,db}(\omega)$ and $\Lambda_{ca,db}(\omega)$ are given by

$$\Gamma_{ca,db}(\omega) = \mathbf{d}_{ca}^* \cdot \boldsymbol{\gamma}(\omega) \cdot \mathbf{d}_{db} \quad (6a)$$

$$\Lambda_{ca,db}(\omega) = \mathbf{d}_{ca}^* \cdot \boldsymbol{\lambda}(\omega) \cdot \mathbf{d}_{db}, \quad (6b)$$

125 where \mathbf{d}_{ca} is a matrix element of the atomic dipole operator, and γ and λ are defined as

$$\gamma(\omega) = 2\pi\mathbf{J}(\omega), \quad (6c)$$

$$\lambda(\omega) = \mathcal{P} \int d\omega' \frac{\mathbf{J}^{\text{scatt}}(\omega')}{\omega - \omega'}. \quad (6d)$$

126 Here, \mathcal{P} denotes the principal value and $\mathbf{J}(\omega)$ is the spectral density of the EM field,

$$\mathbf{J}(\omega) = \frac{\omega^2}{\hbar\pi\epsilon_0 c^2} \text{Im} \mathbf{G}(\mathbf{r}_{\text{at}}, \mathbf{r}_{\text{at}}, \omega). \quad (7)$$

127 We have replaced \mathbf{G} by $\mathbf{G}^{\text{scatt}}$ in $\mathbf{J}^{\text{scatt}}$ (Equation 6d), since the free-space contribution is assumed
 128 to be included in the bare atomic Hamiltonian, and it is also smaller than the NP-induced effects
 129 discussed in this work. We note that while we indicate the complex conjugation of the dipole
 130 matrix elements, it is possible to choose an atomic basis in which they are real; thus, both Γ
 131 and Λ would be real quantities. Note that the expressions for λ contain both the so-called
 132 resonant contributions, which can be shown to be proportional to $\text{Re} \mathbf{G}^{\text{scatt}}$, and non-resonant
 133 contributions to the energy shift [31]. The electromagnetic Green tensor is computed using the
 134 boundary element method implemented in SCUFF-EM [32, 33].

135 Equation 5 does indeed describe the bath-induced interaction between levels, but allows
 136 for non-physical dynamics, as it does not guarantee the positivity of the density matrix. A
 137 standard secularization procedure leads to a completely positive Lindblad equation, but removes
 138 the crucial off-diagonal terms describing state mixing (for more details see subsection A.2
 139 of the appendix). Instead of secularization, we extend the approach of Ref. [19] to obtain a
 140 completely positive Lindblad equation for near-degenerate levels by including the effect of
 141 the counter-rotating terms of the dipolar interaction. This approach consists in replacing both
 142 $\Lambda_{ca,db}(\omega_{bd})$ and $\Lambda_{ca,db}(\omega_{ac})$ with their geometric mean $\tilde{\Lambda}_{ca,db} = \sqrt{\Lambda_{ca,db}(\omega_{bd})\Lambda_{ca,db}(\omega_{ac})}$,
 143 and the same for $\Gamma_{ca,db}(\omega_{bd})$ and $\Gamma_{ca,db}(\omega_{ac})$. Similar ideas have also been proposed elsewhere
 144 in the literature [18, 34]. When applied to Equation 5, this replacement symmetrizes the pairs
 145 of indices ca and db . Then, for the symmetric geometry of Figure 1a where \mathbf{G} is a diagonal
 146 matrix, the resulting master equation can be rewritten as

$$\dot{\rho} = \frac{-i}{\hbar} [H_{\text{at}} + H_{\text{CP}}, \rho] + \sum_{\delta, n} L_{\Sigma_{\delta}^{(n)}}[\rho]. \quad (8)$$

147 Here, H_{CP} is the CP shift, $\Sigma_{\delta}^{(n)}$ are decay operators, and $L_A[\rho] = A\rho A^\dagger - \frac{1}{2}\{A^\dagger A, \rho\}$ is a Lindblad
 148 dissipator. There is a decay operator for each spatial component in the spherical basis $\delta = 0, \pm 1$,
 149 and for each Bohr level n . The CP shift is given by $H_{\text{CP}} = \hbar \sum_{\delta, n} D_{\delta}^{(n)\dagger} D_{\delta}^{(n)}$, where

$$\langle j | D_{\delta}^{(n)} | n \rangle = \sqrt{\lambda_{\delta\delta}(\omega_{nj})} d_{jn}^{\delta}, \quad (9a)$$

150 and the decay operators can be expressed as

$$\langle j | \Sigma_{\delta}^{(n)} | n \rangle = \sqrt{\gamma_{\delta\delta}(\omega_{nj})} d_{jn}^{\delta}. \quad (9b)$$

151 In the definitions above, the atomic states $|n\rangle$ and $|j\rangle$ belong to the n th and j th Bohr level,
 152 respectively. Had the counter-rotating terms in the dipolar coupling not been taken into account,
 153 the Hermitian dipole operators in Equation 5 would have been replaced by raising and lowering
 154 operators, such that only terms where $\omega_j \leq \omega_n$ would be present in Equation 8. Instead, our
 155 description also incorporates the CP shift contribution given by states with $\omega_j > \omega_n$. More
 156 details about the derivation steps can be found in subsection A.3 of the appendix. Finally, we
 157 note that for an atom interacting with a thermal bath, the expression in Equation 8 would

158 contain additional terms proportional to the occupation number $n_T(\omega) = (e^{\hbar\omega/k_B T} - 1)^{-1}$,
 159 but at the relevant transition frequencies this can be shown to be very small for laboratory
 160 temperatures. Therefore, these thermal contributions have been neglected.

161 While solving Equation 8 is considerably more affordable than a direct solution of the
 162 Schrödinger equation with the Hamiltonian from Equation 1, several faithful approximations
 163 allow for further simplification, succinctly described below, with more details and an explicit
 164 check of the validity of the approximations given in Appendix B and Appendix C, respectively.
 165 First, for the dynamics within a single Bohr level, here $n = 7$, we can discard the states with
 166 $n \neq 7$ and write a closed set of equations for $n = 7$, due to the large difference in the energy
 167 scales associated to the Bohr transition energies and the environment-induced perturbations.
 168 The other states are then considered only implicitly as intermediate virtual states that contribute
 169 to the CP and decay terms. Furthermore, within this subspace, the “quantum jump” terms
 170 $\Sigma_\delta^{(7)} \rho \Sigma_\delta^{(7)\dagger}$ in Equation 8 are negligible since they are proportional to $J_{\delta\delta}(\Delta_F)$, and the spectral
 171 density approaches zero for small frequencies. With these approximations, the dynamics within
 172 the $n = 7$ subspace is described by an effective non-Hermitian Hamiltonian

$$H_{\text{eff}}^{(7)} = H_{\text{at}}^{(7)} + \hbar \sum_{\delta} \left(D_{\delta}^{(7)\dagger} D_{\delta}^{(7)} - \frac{i}{2} \Sigma_{\delta}^{(7)\dagger} \Sigma_{\delta}^{(7)} \right), \quad (10)$$

173 where H_{at} has been projected onto the $n = 7$ subspace. Last, due to the axial symmetry of the
 174 system (see Figure 1a), the z component of the total angular momentum is conserved and
 175 Equation 10 consists of independent blocks for each value of m_j . In the following, we focus
 176 on the subspace $m_j = 1/2$, which reduces the number of states to be considered to 7 for this
 177 particular case.

178 3 Results

179 The above derivation significantly simplifies the analysis of the dynamics. In particular, the
 180 effective Hamiltonian can be diagonalized, and the real and imaginary parts of its eigenvalues
 181 correspond to the energies and decay rates of the states including the vacuum-field-induced
 182 state mixing. These energies and decay rates are shown in Figure 2a and Figure 2c, respectively.
 183 Since the CP shift is dominated by an overall attraction to the surface (inset of Figure 2a), we
 184 plot it relative to the average value for each separation d , revealing a completely different and
 185 much more complex structure compared to the fully secularized, diagonal model. In particular,
 186 clear avoided crossings highlight the relevance of the off-diagonal terms, similar to effects found
 187 in interatomic interactions in [35], but here occurring within a single atom. Similarly striking
 188 differences between both models appear in the decay rates shown in Figure 2c. Due to the
 189 off-diagonal terms, the decay rates cross each other several times. Particularly prominent is the
 190 vacuum-field-induced generation of a state that becomes more protected against spontaneous
 191 decay as the atom approaches the NP for separations between about $d = 40$ nm and 60 nm.
 192 This is in stark contrast to the behavior when the states are treated independently, for which
 193 the effect of quenching leads to monotonic increase of the Purcell factor and thus decay rate
 194 with decreasing separation [36, 37]. Here, the same environment that induces the decay also
 195 produces the interactions that mix the states and leads to the formation of a state protected
 196 from the influence of the environment. We note that the subradiant or metastable state created
 197 by field-induced mixing has a smaller decay rate than any of the original eigenstates of the
 198 atom at the same distance when mixing is not included.

199 The emergence of this protected state can be understood by realizing that the system
 200 approaches an idealized situation in which one of the states in the $n = 7$, $m_j = 1/2$ manifold is
 201 fully decoupled from the EM environment. This situation would occur if we could ignore the

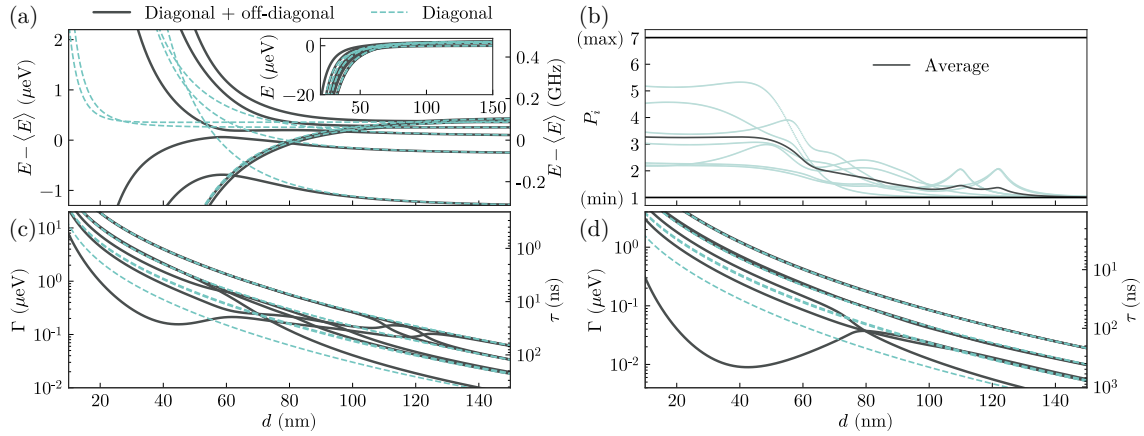


Figure 2: Every quantity is plotted against the atom-NP separation d . (a) Energies of the eigenstates of the effective non-Hermitian Hamiltonian. (b) Participation ratios P_i indicating the degree of mixing of the eigenstates. (c) Decay rates of the eigenstates of the effective non-Hermitian Hamiltonian. (d) Decay rates with the NP shape chosen to optimize the decay rate reduction: $M = 200$ nm and $m = 120$ nm. For plots (a), (c) and (d), the solid black lines correspond to the full model with off-diagonal terms, and the green dashed lines to the model without the off-diagonal terms. For plot (b), the green lines are the participation ratio of each eigenstate, and the black line represents the average participation ratio.

202 (i) fine structure, (ii) x - and y -polarized electric fields in Equation 1, and (iii) contributions of
 203 states outside of the $n = 6$ Bohr level to the CP shift and spontaneous decay. Then, 7 states
 204 in $n = 7$ couple to 6 states in $n = 6$ through the single operator d_z , and there is always one
 205 superposition (“dark state”) with vanishing coupling. For the realistic system, this idealized
 206 situation is approached for various reasons. First, the elongated shape of the NP suppresses the
 207 xx and yy components of J and λ compared to the zz component. Second, the coincidence of
 208 the first peak of J_{zz} and λ_{zz} with the energy of the transition from $n = 7$ to $n = 6$ enhances the
 209 contributions from $n = 6$ intermediate states compared to other Bohr levels. Lastly, when the
 210 CP shifts become greater than the fine structure, the latter becomes a perturbative correction
 211 that can be neglected to lowest order. Based on these considerations, we change the aspect
 212 ratio of the NP by decreasing the minor axis to $m = 120$ nm in order to amplify the protection
 213 of the state. As shown in Figure 2d, the minimum decay rate becomes an order of magnitude
 214 smaller than the naive expectation without off-diagonal terms, unambiguously demonstrating
 215 that the off-diagonal terms can significantly impact the structure of the atom and cannot be
 216 neglected in a realistic description.

217 Next, we evaluate the amount of vacuum-field-induced state mixing. The eigenstates $|\psi\rangle$
 218 of Equation 10 are linear superpositions of the fine structure basis states $|\phi_k\rangle$, and the degree
 219 of this mixing can be quantified using the so-called participation ratio P [38], defined as

$$P(|\psi\rangle) = \left[\sum_k |\langle\psi|\phi_k\rangle|^4 \right]^{-1}. \quad (11)$$

220 It measures the number of basis states “equally” contributing to the normalized state $|\psi\rangle$, with
 221 possible values ranging from 1 to the number of basis states (7 for the case studied here). For
 222 example, for a state of the form $|\psi\rangle = \sqrt{1/n} \sum_{k=1}^n e^{i\theta_k} |\phi_k\rangle$, P equals n . In Figure 2b, we show
 223 the participation ratio of the eigenstates of Equation 10 as a function of the atom-NP separation
 224 d , with green lines showing P for each eigenstate and the thick black line representing the

225 average over all states. We find state mixing to be negligible for separations above ≈ 150 nm,
226 indicating that the off-diagonal contributions to Equation 10 are too small to effectively couple
227 the states. For shorter distances, the magnitude of the off-diagonal terms, $|\langle i|H_{\text{eff}}|j\rangle|$, becomes
228 comparable to the difference of the corresponding diagonal elements, $|\langle i|H_{\text{eff}}|i\rangle - \langle j|H_{\text{eff}}|j\rangle|$,
229 and the states mix appreciably. In particular, clear peaks in P appear when the diagonal CP shifts
230 bring initially detuned states into resonance, such that the off-diagonal elements dominate more
231 easily. Despite the non-monotonic behavior, overall the participation ratios tend to increase
232 as the atom approaches the NP until they stabilize at about $d = 30$ nm. At closer distances,
233 vacuum-field couplings determine the eigenstates and dominate over the fine structure, which
234 becomes a small perturbation of these new eigenstates. We note that for the setup studied here,
235 almost complete mixing of some atomic states is achieved, with values of P larger than 5, close
236 to the theoretical maximum of 7.

237 4 Conclusion

238 In conclusion, we have shown that vacuum-field-induced interactions can significantly mix
239 groups of near-degenerate levels in atoms and must, therefore, be included to accurately
240 characterize the dynamics. We have derived a completely positive Lindblad master equation
241 that provides a precise description of these situations and allows an interpretation of the field-
242 modified atomic structure in terms of an effective non-Hermitian Hamiltonian. For concreteness,
243 we have applied these general ideas to a hydrogen atom coupled to an AlN NP. This leads to
244 striking new features in the atomic structure, such as avoided level crossings and, surprisingly,
245 a decrease of the decay rate for a particular eigenstate with decreasing distance to the NP even
246 though the Purcell factor for each uncoupled state grows monotonically. This illustrates that
247 the off-diagonal terms can even have counterintuitive consequences. Deeper exploration of the
248 eigenstates reveals that the atomic structure in this regime greatly differs from the original fine
249 structure of the free-space atom, even though the atom-field interactions are perturbative and
250 the atom remains a well-defined entity, in contrast to the strong light-matter coupling regime.
251 From an atomic physics' perspective, the hydrogen atom treated here becomes "unrecognizable"
252 as the atomic structure and spectroscopic properties within each sublevel change completely.
253 We note that while we treat a specific setup here, the framework can be straightforwardly
254 applied to other nanostructures (e.g., graphene [10]) and emitters or level splittings (e.g., due
255 to hyperfine structure in Rydberg atoms [35, 39]). Our work thus extends the regime where
256 vacuum-field-induced forces and decay rates are accurately described and opens the door to
257 new strategies for developing quantum state manipulation platforms based on off-diagonal
258 vacuum-induced effects.

259 Acknowledgements

260 **Funding information** This work has been funded by the Spanish Ministry of Science, Innova-
261 tion and Universities-Agencia Estatal de Investigación through the FPI contract No. PRE2019-
262 090589 as well as grants RTI2018-099737-BI00, PID2021-125894NB-I00, and CEX2018-
263 000805-M (through the María de Maeztu program for Units of Excellence in R&D). We
264 also acknowledge financial support from the Proyecto Sinérgico CAM 2020 Y2020/TCS-6545
265 (NanoQuCo-CM) of the Community of Madrid, and from the European Research Council
266 through grant ERC-2016-StG-714870.

267 A Derivation of the master equation

268 The derivation of the Lindblad master equation used in this work, [Equation 8](#), is closely based
 269 on the one presented in [19], modified to include the counter-rotating terms of the light-matter
 270 Hamiltonian and a realistic electromagnetic environment, with three spatial components and
 271 non-trivial structure. We revisit the derivation here and highlight the additions and differences
 272 compared to [19]. For simplicity, the derivation is presented in a way that directly relates to
 273 the illustrative physical system of the main text, that is, a hydrogen atom. However, this is not
 274 a true limitation of the approach and approximations, as long as one considers level structures
 275 with distinct subsets of closely spaced states, a common feature of atomic systems due to fine
 276 structure or hyperfine structure splittings. We start by describing features of the Bloch-Redfield
 277 (BR) equation, and then explain the customary secular approximation, a procedure known
 278 to yield a completely positive Lindblad master equation. This equation would systematically
 279 neglect the off-diagonal terms discussed in this work. Then, we take the BR equation and
 280 perform a series of approximations that lead to a different Lindblad equation, maintaining the
 281 non-secular terms.

282 A.1 Comments on the Bloch-Redfield master equation

283 The BR equation for our system is given by [Equation 5](#). Although it is rather complicated, the
 284 physical interpretation of each line is simple: the first two lines of the sum are responsible for
 285 the Casimir-Polder (CP) shifts, while the third and fourth lines describe decay processes. While
 286 the CP terms can often be neglected, this is not the case for the system we study, as they are
 287 of the same order as the hydrogenic fine structure. For the same reason, we must include the
 288 counter-rotating (CR) terms in the full light-matter Hamiltonian. Otherwise, $\lambda(\omega)$ would only
 289 be evaluated at non-negative frequencies and [Equation 5](#) would miss significant contributions
 290 to the CP terms arising from the negative frequencies. The CR terms only affect the energy shift,
 291 as the decay terms $\gamma(\omega)$ vanish at negative frequencies. It is worth noting that even without
 292 considering the CR terms, the equation already includes the basis for the off-diagonal CP terms
 293 we discuss in the main text, albeit in a complex manner that is hard to disentangle.

294 The BR equation has several drawbacks: First, it does not guarantee positivity of the density
 295 matrix. Although it has been shown that these deviations from physical density matrices are
 296 negligible when the approximations made in deriving the BR equation are valid [21, 40], dealing
 297 with formally unphysical density matrices requires additional care. Second, the BR matrix is
 298 characterized by a superoperator of dimension $N^2 \times N^2$, where N is the number of system
 299 states, which makes analysis of its behavior challenging. In contrast, a Lindblad-type master
 300 equation automatically ensures the physicality of the density matrix, and at the same time
 301 allows for a simpler analysis since it is characterized by a single Hamiltonian and a set of decay
 302 operators, all of dimensions $N \times N$.

303 A.2 Lindblad master equation with full secularization

304 The usual procedure to obtain a Lindblad equation from [Equation 5](#) is the so-called secular
 305 approximation which consists in eliminating every term where $\omega_{ac} \neq \omega_{bd}$. Doing so yields

$$\begin{aligned} \dot{\rho} = & -\frac{i}{\hbar} [H_{\text{at}}, \rho] - i \sum_{abd}^{(S)} [\Lambda_{da,db}(\omega_{bd}) |a\rangle\langle b|, \rho] \\ & + \sum_{abcd}^{(S)} \Gamma_{ca,db}(\omega_{bd}) \left(|d\rangle\langle b| \rho |a\rangle\langle c| - \frac{1}{2} \{ |a\rangle\langle c| d\rangle\langle b|, \rho \} \right) \end{aligned} \quad (12)$$

306 where the superscript (S) in the sum indicates that only terms with $\omega_{ac} = \omega_{bd}$ are kept. In the
 307 energy shift, this is equivalent to the condition $\omega_a = \omega_b$ since $|c\rangle = |d\rangle$ there. The energy shift is
 308 clearly Hermitian because it is a real and symmetric matrix. The decay term can be reexpressed
 309 by grouping the sum over transitions into sets with a given frequency $\Omega = \omega_{ac} = \omega_{bd}$, which
 310 yields

$$\sum_{\Omega} \sum_{\alpha\beta} \gamma_{\alpha\beta}(\Omega) \left(\sigma_{\Omega}^{\beta} \rho \sigma_{\Omega}^{\alpha\dagger} - \frac{1}{2} \{ \sigma_{\Omega}^{\alpha\dagger} \sigma_{\Omega}^{\beta}, \rho \} \right) = \sum_{\Omega\epsilon} \Gamma_{\epsilon}(\Omega) \left(S_{\Omega}^{\epsilon} \rho S_{\Omega}^{\epsilon\dagger} - \frac{1}{2} \{ S_{\Omega}^{\epsilon\dagger} S_{\Omega}^{\epsilon}, \rho \} \right). \quad (13)$$

311 Here, Greek indices α, β indicate spatial directions, while all dipole transitions d^{α} with a
 312 frequency difference of Ω are combined in the transition operators $\sigma_{\Omega}^{\alpha} = \sum_{ab}^{(\Omega)} d_{ab}^{\alpha} |a\rangle\langle b|$. The
 313 right-hand side above is obtained by diagonalizing the positive definite matrix $\gamma_{\alpha\beta}(\Omega) =$
 314 $\sum_{\epsilon} M_{\alpha\epsilon}^{\dagger}(\Omega) \Gamma_{\epsilon}(\Omega) M_{\epsilon\beta}(\Omega)$ for each transition frequency Ω and defining $S_{\Omega}^{\epsilon} = \sum_{\alpha} M_{\epsilon\alpha}(\Omega) \sigma_{\Omega}^{\alpha}$.
 315 In this last form, it is evident that the full secularization returns a Lindblad master equation.
 316 However, the only off-diagonal terms present are the ones connecting degenerate states. This
 317 approximation has been shown to be inadequate in a variety of contexts [19, 21, 40], since it
 318 indiscriminately removes the coupling between coherences (off-diagonal elements of ρ) and
 319 populations of non-degenerate states. Thus, in the system explored in the main text, relevant
 320 physics would be omitted within each Bohr level.

321 A.3 Lindblad master equation: derivation details and proof

322 We here show how to derive the Lindblad equation including off-diagonal terms between
 323 non-degenerate states used in the main text from the BR equation, Equation 5. Instead of
 324 a full secularization as discussed above, we start by performing a partial secularization to
 325 discard terms where the timescale induced by the environment, $\tau_E \sim \min(|\mathbf{d}^2\lambda|^{-1}, |\mathbf{d}^2\gamma|^{-1})$, is
 326 much larger than that of the atomic transitions, $\tau_{at} \sim |\omega_{ac} - \omega_{bd}|^{-1}$. This is not an important
 327 step, but it significantly simplifies the resulting expressions. In Equation 5, this is fulfilled for
 328 terms where $|a\rangle$ and $|b\rangle$ belong to different Bohr levels: First, if either $|c\rangle$ or $|d\rangle$ belongs to a
 329 different Bohr level than $|a\rangle$ and $|b\rangle$, respectively, then τ_{at} is very small compared with τ_E ,
 330 and secularization is well-justified. If, instead, $|c\rangle$ and $|d\rangle$ belong to the same Bohr levels as
 331 $|a\rangle$ and $|b\rangle$, respectively, then $\tau_E \propto 1/\gamma(\Delta_F/\hbar)$ becomes extremely large because Δ_F is on the
 332 scale of the fine structure splitting and the spectral density approaches 0 when ω goes to 0.
 333 Hence, even if $\tau_{at} \sim \hbar/\Delta_F$ is large, τ_E is even larger in the system studied here. This partially
 334 secularized BR equation is significantly simpler than the full one, but is not yet in Lindblad
 335 form.

336 We next apply the geometric mean replacement discussed in the main text to Equation 5
 337 and obtain

$$\begin{aligned} \dot{\rho} = & -\frac{i}{\hbar} [H_{at}, \rho] - i \left[\sum_{abcd}^{(s)} \tilde{\Lambda}_{ca,db} |a\rangle\langle c|d\rangle\langle b|, \rho \right] \\ & + \sum_{abcd}^{(s)} \tilde{\Gamma}_{ca,db} \left(|d\rangle\langle b|\rho|c\rangle\langle a| - \frac{1}{2} \{ |a\rangle\langle c|d\rangle\langle b|, \rho \} \right), \end{aligned} \quad (14)$$

338 where the superscript (s) in the sum indicates the partial secularization mentioned above.
 339 This procedure is accurate for the following reason. When the spectral density, given in
 340 Equation 7, is slowly varying: $J(\omega + |\mathbf{d}^2\lambda|) \simeq J(\omega)$ and $J(\omega + |\mathbf{d}^2\gamma|) \simeq J(\omega)$. In that case,
 341 for each term in Equation 5 where $|\omega_{ac} - \omega_{bd}| < \max(|\mathbf{d}^2\gamma|, |\mathbf{d}^2\lambda|)$, the change in the value
 342 of the element is small, and the geometric mean is a good approximation. For terms where
 343 $|\omega_{ac} - \omega_{bd}| > \max(|\mathbf{d}^2\gamma|, |\mathbf{d}^2\lambda|)$, the value might change appreciably, but its effect on the

344 dynamics is small due to the difference in energy scales. In fact, such terms could be eliminated
345 through an additional secularization to a good approximation.

346 After the replacement, the CP Hamiltonian, $H_{\text{CP}} = \hbar \sum_{abc}^{(s)} \tilde{\Lambda}_{ca,cb} |a\rangle\langle b|$, contains both diago-
347 nal and off-diagonal matrix elements. We note that the effect of the CR terms of the light-matter
348 coupling is manifested in the precise values of the matrix elements, which change significantly
349 depending on whether the CR interactions are included or not. Careful analysis shows that
350 this Hamiltonian is Hermitian if $\lambda(\omega_{ca})$ and $\lambda(\omega_{bd})$ have the same sign. Since $\lambda(\omega)$ has sign
351 changes, in general, this is not always necessarily satisfied, leading to a potentially problematic,
352 non-Hermitian CP Hamiltonian. In the cases studied in the manuscript, the partial secular-
353 ization we performed earlier ensures that only terms with $\omega_{ac} \simeq \omega_{bc}$ survive, and combined
354 with the slow-varying property of the spectral density, the sign condition is satisfied always.
355 A discussion of the general situation where this is not necessarily true will be presented in a
356 future work.

357 In order for Equation 14 to be a Lindblad-type master equation, the decay rate tensor $\tilde{\Gamma}_{ca,db}$
358 interpreted as a matrix in the combined indices ca and db , sometimes called Kossakovski matrix,
359 has to be positive semidefinite. Then, it can be diagonalized with non-negative eigenvalues and
360 the last term in Equation 14 can be rewritten as a sum of standard Lindblad decay terms. While
361 it is symmetric by construction, we are not aware of a general proof of positive semidefiniteness
362 of the decay tensor that results when the procedure described above is applied to arbitrary
363 spectral densities and atomic spectra. For the cases we treat in the manuscript, where the
364 Green tensor is diagonal and cylindrically symmetric such that its Cartesian components satisfy
365 $G_{xx} = G_{yy}$, we give a proof below through explicit construction of the diagonalized form.
366 Under this assumption, the decay tensor has the form $\gamma(\omega) = \text{diag}(\gamma_{xx}(\omega), \gamma_{yy}(\omega), \gamma_{zz}(\omega))$.
367 We now express $\Gamma_{ca,db}(\omega)$ in terms of the spherical basis defined by

$$\mathbf{d}' = \begin{bmatrix} d^{+1} \\ d^{-1} \\ d^0 \end{bmatrix} = \mathbf{U} \cdot \mathbf{d} = \begin{bmatrix} -1/\sqrt{2} & -i/\sqrt{2} & 0 \\ 1/\sqrt{2} & -i/\sqrt{2} & 0 \\ 0 & 0 & 1 \end{bmatrix} \cdot \begin{bmatrix} d^x \\ d^y \\ d^z \end{bmatrix}. \quad (15)$$

368 By construction, the spherical components of the dipole operator, d^δ , connect states with a
369 given m_j to states with $m_j + \delta$. Due to its symmetry, $\gamma(\omega)$ is invariant under transformation to
370 the spherical basis, $\gamma'(\omega) = \mathbf{U} \cdot \gamma(\omega) \cdot \mathbf{U}^\dagger = \gamma(\omega)$. Since m_j is a well-defined quantum number
371 of our basis states, the advantage of the spherical basis is that every transition operator $|a\rangle\langle c|$
372 allowed by the selection rules (see Fig. 1b of the main text) is mediated by only one of d^{+1} ,
373 d^{-1} or d^0 . Furthermore, because of the diagonal form of γ' , the transition operators $|d\rangle\langle b|$ and
374 $|c\rangle\langle a|$ must have the same δ ; otherwise $\Gamma_{ca,db}(\omega) = 0$. As a consequence, we can expand the
375 last term of Equation 14 as three separate sums, one for each value of δ , indicated below with
376 the label δ on the second summation sign:

$$\begin{aligned} & \sum_{\delta} \sum_{abcd}^{(s,\delta)} \sqrt{\Gamma_{ac,db}(\omega_{bd})} \sqrt{\Gamma_{ac,db}(\omega_{ac})} \left[|d\rangle\langle b| \rho |a\rangle\langle c| - \frac{1}{2} \{ |a\rangle\langle c| d \rangle\langle b|, \rho \} \right] = \\ & \sum_{\delta} \sum_{abcd}^{(s,\delta)} d_{ca}^{\delta*} d_{db}^{\delta} \sqrt{\gamma_{\delta\delta}(\omega_{bd})} \sqrt{\gamma_{\delta\delta}(\omega_{ac})} \left[|d\rangle\langle b| \rho |a\rangle\langle c| - \frac{1}{2} \{ |a\rangle\langle c| d \rangle\langle b|, \rho \} \right] = \\ & \sum_{\delta n} \left(\Sigma_{\delta}^{(n)} \rho \Sigma_{\delta}^{(n)\dagger} - \frac{1}{2} \{ \Sigma_{\delta}^{(n)\dagger} \Sigma_{\delta}^{(n)}, \rho \} \right), \end{aligned} \quad (16)$$

377 where we have used that $\gamma_{\delta\delta}(\omega) > 0$ and that the d_{ca}^{δ} are real for any pair ca , and in the last
378 step, we have defined the summed transition operator

$$\Sigma_{\delta}^{(n)} = \sum_{db}^{(n)} d_{db}^{\delta} \sqrt{\gamma_{\delta\delta}(\omega_{bd})} |d\rangle\langle b|. \quad (17a)$$

379 Here, the states $|b\rangle$ belong to the same Bohr level with main quantum number equal to n , while
 380 the $|d\rangle$ states can belong to any Bohr level. This simplification is a consequence of the partial
 381 secularization explained at the beginning of this subsection. In this form, the decay term is
 382 given by an explicit Lindblad operator in terms of just three decay operators for each Bohr level
 383 n . We note that identical manipulations can be done on the energy shift terms, which can be
 384 refactored as

$$D_{\delta}^{(n)} = \sum_{db}^{(n)} d_{db}^{\delta} \sqrt{\lambda_{\delta\delta}(\omega_{bd})} |d\rangle\langle b|. \quad (17b)$$

385 Finally, we can rewrite Equation 14 in our system as

$$\dot{\rho} = -\frac{i}{\hbar} [H_{\text{at}} + H_{\text{CP}}, \rho] + \sum_{\delta n} L_{\Sigma_{\delta}^{(n)}}[\rho] \quad (18)$$

386 where $H_{\text{CP}} = \hbar \sum_{\delta n} D_{\delta}^{(n)\dagger} D_{\delta}^{(n)}$ and $L_A[\rho] = A\rho A^{\dagger} - \frac{1}{2}\{A^{\dagger}A, \rho\}$ is a standard Lindblad decay term.
 387 This is indeed a Lindblad equation for the atom that includes the relevant off-diagonal couplings
 388 both in the CP shift and the decay term.

389 B Derivation of the effective Hamiltonian

390 Any Lindblad equation $\dot{\rho} = -\frac{i}{\hbar} [H, \rho] + \sum_j L_{A_j}[\rho]$ can be rewritten as $\dot{\rho} = -\frac{i}{\hbar} (H_{\text{eff}}\rho - \rho H_{\text{eff}}^{\dagger}) +$
 391 $\sum_j A_j \rho A_j^{\dagger}$, with the effective non-Hermitian Hamiltonian $H_{\text{eff}} = H - \frac{i}{2} \sum_j A_j^{\dagger} A_j$, and the terms
 392 of the last sum commonly referred to as the “refilling” or “quantum jump” terms. In physical
 393 situations where the refilling terms are negligible, the dynamics are then fully characterized by
 394 the eigenstates and eigenvalues of the effective Hamiltonian [41]. In the main text, we are
 395 concerned with the dynamics within a given Bohr level, in particular $n = 7$. Due to the partial
 396 secularization we performed, the effective Hamiltonian associated with Equation 18 is block-
 397 diagonal in Bohr levels, such that n remains a good quantum number and $[H_{\text{eff}}, \mathcal{P}_n] = 0$, where
 398 \mathcal{P}_n is a projection operator onto the subspace with principal quantum number n . Projecting the
 399 Lindblad master equation onto this subspace gives

$$\dot{\rho}_n = -\frac{i}{\hbar} (H_{\text{eff}}^{(n)} \rho_n - \rho_n H_{\text{eff}}^{(n)\dagger}) + \sum_{\delta n'} \mathcal{P}_n \Sigma_{\delta}^{(n')} \rho \Sigma_{\delta}^{(n')\dagger} \mathcal{P}_n, \quad (19)$$

$$H_{\text{eff}}^{(n)} = \mathcal{P}_n H_{\text{eff}} \mathcal{P}_n = H_{\text{at}}^{(n)} + \hbar \sum_{\delta} \left(D_{\delta}^{(n)\dagger} D_{\delta}^{(n)} - \frac{i}{2} \Sigma_{\delta}^{(n)\dagger} \Sigma_{\delta}^{(n)} \right), \quad (20)$$

400 where $\rho_n = \mathcal{P}_n \rho \mathcal{P}_n$ and $H_{\text{at}}^{(n)} = \mathcal{P}_n H_{\text{at}} \mathcal{P}_n$. We thus only need to show that the refilling terms
 401 are negligible for the dynamics within a given Bohr level. To this end, we can rewrite them as

$$\mathcal{P}_n \Sigma_{\delta}^{(n')} \rho \Sigma_{\delta}^{(n')\dagger} \mathcal{P}_n = \sum_{abcd}^{(s,\delta)} d_{ca}^{\delta*} d_{db}^{\delta} \sqrt{\gamma_{\delta\delta}(\omega_{bd})} \sqrt{\gamma_{\delta\delta}(\omega_{ac})} \mathcal{P}_n |d\rangle\langle b| \rho |a\rangle\langle c| \mathcal{P}_n. \quad (21)$$

402 Because of the partial secular approximation, $|a\rangle$ and $|b\rangle$ belong to the same Bohr level n' ,
 403 and due to the projection operators \mathcal{P}_n , $|c\rangle$ and $|d\rangle$ also have the same principal quantum
 404 number, n . Also, because γ is only non-zero at positive frequencies, we have that $n' \geq n$. We
 405 can immediately discard terms with $n' > n$: They refer to the population that flows into the
 406 Bohr level n through spontaneous emission from higher-lying Bohr levels, but since we assume
 407 that the initial atomic state is in level n and there are no processes leading to higher levels,
 408 these terms do not contribute. For the remaining terms with $n' = n$, the atomic time scales

409 are $\tau_{\text{at}} \sim \hbar/\Delta_F$, but the decay-induced time scales are $\tau_E \propto 1/\gamma(\Delta_F/\hbar)$. Given the spectral
 410 density used in the main text, in our system $\tau_E \gg \tau_{\text{at}}$. Thus, the effect of the terms with $n' = n$
 411 is negligible, and we can safely remove the “refilling” term and write the dynamics in the
 412 subspace with principal quantum number n as

$$\dot{\rho}_n = -\frac{i}{\hbar} \left(H_{\text{eff}}^{(n)} \rho_n - \rho_n H_{\text{eff}}^{(n)\dagger} \right), \quad (22)$$

413 which is equivalent to the Schrödinger equation $\partial_t |\psi(t)\rangle = -\frac{i}{\hbar} H_{\text{eff}}^{(n)} |\psi(t)\rangle$.

414 B.1 Angular momentum conservation

415 For each Bohr level n , the effective Hamiltonian Equation 20 derived above is a block diagonal
 416 matrix, with each block corresponding to a given value of the z -projection m_j of the atomic
 417 angular momentum. This is easy to see since H_{at} conserves angular momentum, while the
 418 operators $D_{\delta}^{(n)}$ and $\Sigma_{\delta}^{(n)}$ connect m_j to $m_j + \delta$, and their Hermitian conjugates connect $m_j + \delta$
 419 back to m_j , such that overall, m_j is conserved. In contrast, physically and in the full Lindblad
 420 master equation Equation 18, it is only the z -projection of the total angular momentum of the
 421 photons and atom together that is conserved due to the cylindrical symmetry of the system.
 422 Indeed, the complete master equation in Equation 18 does connect different m_j subspaces
 423 through the refilling term. Since we have shown this term to be negligible for the dynamics
 424 within a given subspace, we can exploit conservation of m_j to analyze its subspaces separately,
 425 and have done so in the main text by fixing $m_j = 1/2$.

426 C Numerical check

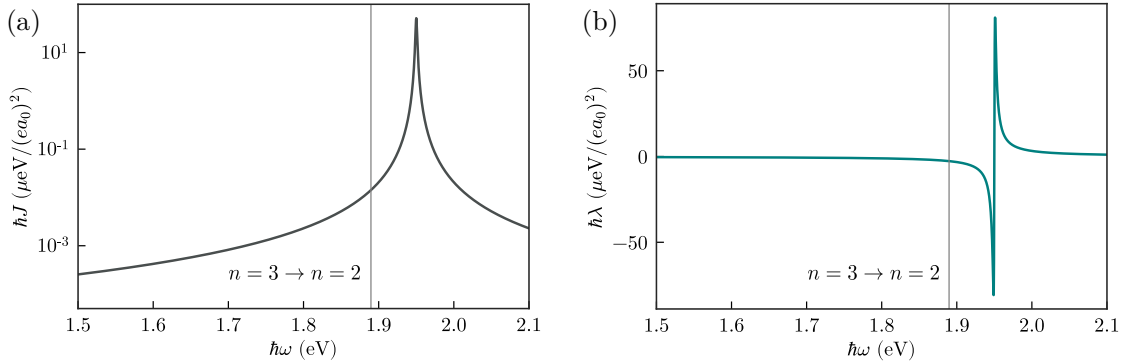


Figure 3: (a) Model spectral density, $J(\omega)$. (b) Integral of the spectral density that appears in the shift, $\lambda(\omega)$.

427 In order to verify the validity of the derived Lindblad equation and effective Hamiltonian,
 428 we here apply it to a simplified system for which an exact solution is possible. To do so, we study
 429 the populations of the states with $n = 3$ in the hydrogen atom coupled to an electromagnetic
 430 bath whose spectral density is a Lorentzian. The density and the corresponding energy shift

431 integral are shown in [Figure 3a](#) and [Figure 3b](#), and are given by

$$J(\omega) = \frac{g^2}{\pi} \frac{\kappa/2}{(\omega - \omega_M)^2 + (\kappa/2)^2}, \quad (23)$$

$$\lambda(\omega) = \int_{-\infty}^{\infty} d\omega' \frac{J(\omega')}{\omega - \omega'} = g^2 \frac{\omega - \omega_M}{(\omega - \omega_M)^2 + (\kappa/2)^2}, \quad (24)$$

432 with parameter values $\hbar g = (9/\sqrt{5}) \cdot 10^{-4}$ eV/(ea_0), $\hbar\kappa = 2 \cdot 10^{-3}$ eV and $\hbar\omega_M = 1.95$ eV.
 433 It is well-known that a Lorentzian spectral density is completely equivalent to a single mode
 434 coupled to a completely flat, i.e. Markovian, bath [[42](#), [43](#)], with dynamics described exactly by
 435 a Lindblad equation [[44](#)],

$$\dot{\rho} = -\frac{i}{\hbar} [H_{\text{at}} + \hbar\omega_M a^\dagger a, \rho] - \frac{\kappa}{2} \{a^\dagger a, \rho\} + \kappa a \rho a^\dagger, \quad (25)$$

436 where a is the bosonic annihilation operator of the bath mode. Hence, we can compare the
 437 approximate solutions obtained with our approaches, [Equation 18](#) and [Equation 22](#), to the exact
 438 dynamics given by [Equation 25](#). We take $|\psi(0)\rangle = |n=3, l=0, j=1/2, m_j=1/2\rangle |n_{\text{ph}}=0\rangle$ as
 the initial state and propagate it in time.

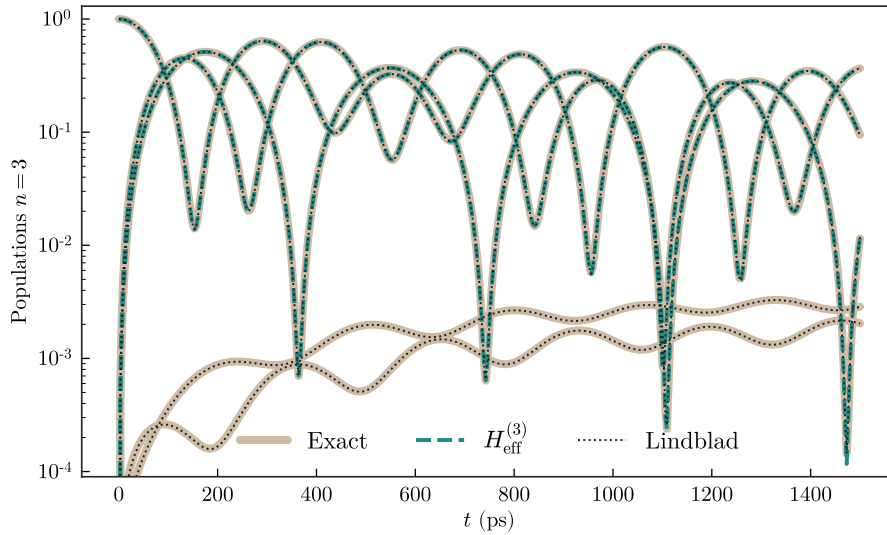


Figure 4: Time evolution of the atomic populations. Thick brown lines: numerical solution to the exact dynamics ([Equation 25](#)). Green dashed lines: effective Hamiltonian ([Equation 22](#)). Black dotted lines: Lindblad master equation ([Equation 18](#)).

439

440 In the exact calculations, we include the first 4 Bohr levels of the hydrogen atom with
 441 their complete fine structure (60 states), which gives converged results. The population of
 442 the $|3, l, j, 1/2\rangle$ states are plotted in [Figure 4](#). The three largest populations are perfectly well
 443 described by both our Lindblad equation and the effective, non-Hermitian Hamiltonian. It
 444 should be noted that the dynamics calculated using the BR approach are essentially the same
 445 as those obtained from the Lindblad equation and therefore not shown separately. There are
 446 two additional lines that are present only in the exact dynamics and the Lindblad equation,
 447 with populations of the order of 10^{-3} . These are states that become populated through the
 448 refilling terms within the $n=3$ subspace discussed above. These are unrealistically large here
 449 because the spectral density chosen here to enable comparison with an exact result does not
 450 obey the physical constraint $J(\omega) = 0$ for $\omega \leq 0$. In contrast, the spectral density used in the

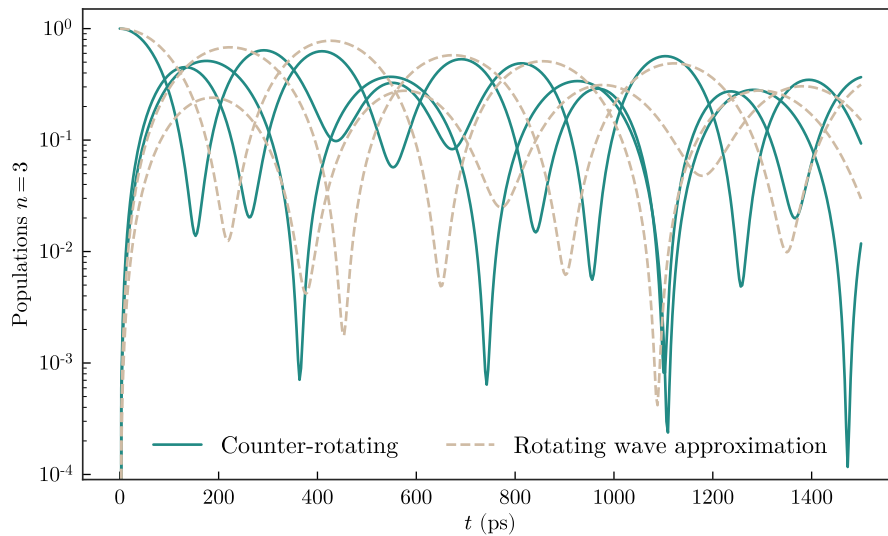


Figure 5: Dynamics calculated with the effective Hamiltonian. Green lines: including the contribution of the CR terms. Brown dashed lines: the rotating wave approximation has been performed on the light-matter Hamiltonian.

451 main text obeys these physical constraints and the refilling term can indeed be discarded with
 452 much less impact.

453 Having checked the validity of Equation 20, we may use it to reinforce the claim that the
 454 CR terms are important in our work. In Figure 5, we compare the dynamics when the effect of
 455 the CR terms is included and when it is not due to the rotating wave approximation. Clearly,
 456 the marked differences in the oscillations indicates that the CR terms significantly contribute to
 457 the CP shift and thus to the dynamics.

458 References

- 459 [1] P. W. Milonni, *The quantum vacuum: an introduction to quantum electrodynamics*, Academic
 460 Press, doi:[10.1016/C2009-0-21295-5](https://doi.org/10.1016/C2009-0-21295-5) (1994).
- 461 [2] E. M. Purcell, *Spontaneous emission probabilities at radio frequencies*, Phys. Rev. **69**, 681
 462 (1946), doi:[10.1103/PhysRev.69.674.2](https://doi.org/10.1103/PhysRev.69.674.2).
- 463 [3] S. Y. Buhmann, *Dispersion Forces I: Macroscopic Quantum Electrodynamics and Ground-
 464 State Casimir, Casimir-Polder and van der Waals Forces*, Springer Berlin Heidelberg, ISBN
 465 978-3-642-32484-0, doi:[10.1007/978-3-642-32484-0](https://doi.org/10.1007/978-3-642-32484-0) (2012).
- 466 [4] D. Press, S. Götzinger, S. Reitzenstein, C. Hofmann, A. Löffler, M. Kamp, A. Forchel
 467 and Y. Yamamoto, *Photon antibunching from a single quantum-dot-microcavity
 468 system in the strong coupling regime*, Phys. Rev. Lett. **98**, 117402 (2007),
 469 doi:[10.1103/PhysRevLett.98.117402](https://doi.org/10.1103/PhysRevLett.98.117402).
- 470 [5] I. Aharonovich, D. Englund and M. Toth, *Solid-state single-photon emitters*, Nature
 471 Photonics **10**, 631 (2016), doi:[10.1038/nphoton.2016.186](https://doi.org/10.1038/nphoton.2016.186).
- 472 [6] T. D. Barrett, T. H. Doherty and A. Kuhn, *Pushing purcell enhancement beyond its limits*,
 473 New Journal of Physics **22**(6), 063013 (2020), doi:[10.1088/1367-2630/ab8ab0](https://doi.org/10.1088/1367-2630/ab8ab0).

- 474 [7] G. Binnig, C. F. Quate and C. Gerber, *Atomic force microscope*, Phys. Rev. Lett. **56**, 930
475 (1986), doi:[10.1103/PhysRevLett.56.930](https://doi.org/10.1103/PhysRevLett.56.930).
- 476 [8] C. Stehle, H. Bender, C. Zimmermann, D. Kern, M. Fleischer and S. Slama, *Plasmoni-*
477 *cally tailored micropotentials for ultracold atoms*, Nature Photonics **5**(8), 494 (2011),
478 doi:[10.1038/nphoton.2011.159](https://doi.org/10.1038/nphoton.2011.159).
- 479 [9] J. D. Thompson, T. G. Tiecke, N. P. de Leon, J. Feist, A. V. Akimov, M. Gullans, A. S. Zibrov,
480 V. Vuletić and M. D. Lukin, *Coupling a Single Trapped Atom to a Nanoscale Optical Cavity*,
481 Science **340**, 1202 (2013), doi:[10.1126/science.1237125](https://doi.org/10.1126/science.1237125).
- 482 [10] C.-H. Chang, N. Rivera, J. D. Joannopoulos, M. Soljačić and I. Kaminer, *Constructing*
483 *“designer atoms” via resonant graphene-induced Lamb shifts*, ACS Photonics **4**(12), 3098
484 (2017), doi:[10.1021/acsp Photonics.7b00731](https://doi.org/10.1021/acsp Photonics.7b00731).
- 485 [11] H.-P. Breuer and F. Petruccione, *The theory of open quantum systems*, Oxford University
486 Press, doi:[10.1093/acprof:oso/9780199213900.001.0001](https://doi.org/10.1093/acprof:oso/9780199213900.001.0001) (2002).
- 487 [12] S. Ribeiro, S. Y. Buhmann, T. Stielow and S. Scheel, *Casimir-Polder interaction from*
488 *exact diagonalization and surface-induced state mixing*, EPL **110**(5), 51003 (2015),
489 doi:[10.1209/0295-5075/110/51003](https://doi.org/10.1209/0295-5075/110/51003).
- 490 [13] S. Y. Buhmann, L. Knöll, D.-G. Welsch and H. T. Dung, *Casimir-polder forces: A nonpertur-*
491 *bative approach*, Phys. Rev. A **70**, 052117 (2004), doi:[10.1103/PhysRevA.70.052117](https://doi.org/10.1103/PhysRevA.70.052117).
- 492 [14] S. Y. Buhmann and D.-G. Welsch, *Casimir-polder forces on excited atoms in the strong atom-*
493 *field coupling regime*, Phys. Rev. A **77**, 012110 (2008), doi:[10.1103/PhysRevA.77.012110](https://doi.org/10.1103/PhysRevA.77.012110).
- 494 [15] D. A. Cardimona, M. G. Raymer and C. R. S. Jr, *Steady-state quantum interference in*
495 *resonance fluorescence*, Journal of Physics B: Atomic and Molecular Physics **15**(1), 55
496 (1982), doi:[10.1088/0022-3700/15/1/012](https://doi.org/10.1088/0022-3700/15/1/012).
- 497 [16] D. A. Cardimona and C. R. Stroud, *Spontaneous radiative coupling of atomic energy levels*,
498 Phys. Rev. A **27**, 2456 (1983), doi:[10.1103/PhysRevA.27.2456](https://doi.org/10.1103/PhysRevA.27.2456).
- 499 [17] M. Donaire, M.-P. Gorza, A. Maury, R. Guérout and A. Lambrecht, *Casimir-polder-induced*
500 *rabi oscillations*, Europhysics Letters **109**(2), 24003 (2015), doi:[10.1209/0295-](https://doi.org/10.1209/0295-5075/109/24003)
501 [5075/109/24003](https://doi.org/10.1209/0295-5075/109/24003).
- 502 [18] Z. Ficek and S. Swain, *Quantum interference and coherence: theory and experiments*, vol.
503 100, Springer Science & Business Media (2005).
- 504 [19] G. McCauley, B. Cruikshank, D. I. Bondar and K. Jacobs, *Accurate Lindblad-form master*
505 *equation for weakly damped quantum systems across all regimes*, npj Quantum Information
506 **6**, 74 (2020), doi:[10.1038/s41534-020-00299-6](https://doi.org/10.1038/s41534-020-00299-6).
- 507 [20] D. Manzano, *A short introduction to the Lindblad master equation*, AIP Adv. **10**(2), 025106
508 (2020), doi:[10.1063/1.5115323](https://doi.org/10.1063/1.5115323).
- 509 [21] P. R. Eastham, P. Kirton, H. M. Cammack, B. W. Lovett and J. Keeling, *Bath-*
510 *induced coherence and the secular approximation*, Phys. Rev. A **94**(1), 012110 (2016),
511 doi:[10.1103/PhysRevA.94.012110](https://doi.org/10.1103/PhysRevA.94.012110).
- 512 [22] B. Huttner and S. M. Barnett, *Quantization of the electromagnetic field in dielectrics*, Phys.
513 Rev. A **46**, 4306 (1992), doi:[10.1103/PhysRevA.46.4306](https://doi.org/10.1103/PhysRevA.46.4306).

- 514 [23] W. Vogel and D. Welsch, *Quantum Optics*, Wiley, 1 edn., ISBN 978-3-527-40507-7
515 978-3-527-60852-2, doi:[10.1002/3527608524](https://doi.org/10.1002/3527608524) (2006).
- 516 [24] S. Scheel and S. Y. Buhmann, *Macroscopic quantum electrodynamics - Concepts and*
517 *applications*, Acta Physica Slovaca **58**(5) (2008).
- 518 [25] E. A. Power and S. Zienau, *Coulomb gauge in non-relativistic quantum electrodynamics*
519 *and the shape of spectral lines*, Philos. Trans. R. Soc. Lond. Ser. A **251**, 427 (1959),
520 doi:[10.1098/rsta.1959.0008](https://doi.org/10.1098/rsta.1959.0008).
- 521 [26] R. G. Woolley, *Molecular quantum electrodynamics*, Proc. R. Soc. Lond. Ser. A **321**, 557
522 (1971), doi:[10.1098/rspa.1971.0049](https://doi.org/10.1098/rspa.1971.0049).
- 523 [27] R. G. Woolley, *Gauge invariance in non-relativistic electrodynamics*, Proceedings of the
524 Royal Society A: Mathematical, Physical and Engineering Sciences **456**(2000), 1803
525 (2000), doi:[10.1098/rspa.2000.0587](https://doi.org/10.1098/rspa.2000.0587).
- 526 [28] C. Cohen-Tannoudji, B. Diu and F. Laloe, *Quantum mechanics Vol.2*, Wiley-Interscience,
527 New York (1978).
- 528 [29] S. Foteinopoulou, G. C. R. Devarapu, G. S. Subramania, S. Krishna and D. Wasserman,
529 *Phonon-polaritons: enabling powerful capabilities for infrared photonics*, Nanophotonics
530 **12**, 2129 (2019), doi:[10.1515/nanoph-2019-0232](https://doi.org/10.1515/nanoph-2019-0232).
- 531 [30] C. Cohen-Tannoudji, G. Grynberg and J. Dupont-Roc, *Atom-Photon Interactions: Basic*
532 *Processes and Applications*, Wiley (1992).
- 533 [31] S. Y. Buhmann, *Dispersion Forces II: Many-Body Effects, Excited Atoms, Finite Temper-*
534 *ature and Quantum Friction*, Springer Berlin Heidelberg, ISBN 978-3-642-32465-9,
535 doi:[10.1007/978-3-642-32466-6](https://doi.org/10.1007/978-3-642-32466-6) (2012).
- 536 [32] M. T. H. Reid and S. G. Johnson, *Efficient computation of power, force, and torque in beam*
537 *scattering calculations*, IEEE Transactions on Antennas and Propagation **63**(8), 3588
538 (2015), doi:[10.1109/TAP.2015.2438393](https://doi.org/10.1109/TAP.2015.2438393).
- 539 [33] <https://github.com/HomerReid/scuff-EM>.
- 540 [34] D. Davidović, *Completely Positive, Simple, and Possibly Highly Accurate Approximation of*
541 *the Redfield Equation*, Quantum **4**, 326 (2020), doi:[10.22331/q-2020-09-21-326](https://doi.org/10.22331/q-2020-09-21-326).
- 542 [35] J. Block and S. Scheel, *Casimir-polder-induced rydberg macrodimers*, Phys. Rev. A **100**,
543 062508 (2019), doi:[10.1103/PhysRevA.100.062508](https://doi.org/10.1103/PhysRevA.100.062508).
- 544 [36] P. Anger, P. Bharadwaj and L. Novotny, *Enhancement and quenching of single-molecule*
545 *fluorescence*, Phys. Rev. Lett. **96**, 113002 (2006), doi:[10.1103/PhysRevLett.96.113002](https://doi.org/10.1103/PhysRevLett.96.113002).
- 546 [37] S. Kühn, U. Håkanson, L. Rogobete and V. Sandoghdar, *Enhancement of single-molecule*
547 *fluorescence using a gold nanoparticle as an optical nanoantenna*, Phys. Rev. Lett. **97**,
548 017402 (2006), doi:[10.1103/PhysRevLett.97.017402](https://doi.org/10.1103/PhysRevLett.97.017402).
- 549 [38] B. Kramer and A. MacKinnon, *Localization: theory and experiment*, Reports on Progress
550 in Physics **56**(12), 1469 (1993), doi:[10.1088/0034-4885/56/12/001](https://doi.org/10.1088/0034-4885/56/12/001), Publisher: IOP
551 Publishing.
- 552 [39] T. G. Walker and M. Saffman, *Consequences of zeeman degeneracy for the van*
553 *der waals blockade between rydberg atoms*, Phys. Rev. A **77**, 032723 (2008),
554 doi:[10.1103/PhysRevA.77.032723](https://doi.org/10.1103/PhysRevA.77.032723).

- 555 [40] J. Jeske, D. J. Ing, M. B. Plenio, S. F. Huelga and J. H. Cole, *Bloch-Redfield equa-*
556 *tions for modeling light-harvesting complexes*, J. Chem. Phys. **142**(6), 064104 (2015),
557 doi:[10.1063/1.4907370](https://doi.org/10.1063/1.4907370).
- 558 [41] P. M. Visser and G. Nienhuis, *Solution of Quantum Master Equations in*
559 *Terms of a Non-Hermitian Hamiltonian*, Phys. Rev. A **52**(6), 4727 (1995),
560 doi:[10.1103/PhysRevA.52.4727](https://doi.org/10.1103/PhysRevA.52.4727).
- 561 [42] A. Imamoglu, *Stochastic wave-function approach to non-markovian systems*, Phys. Rev. A
562 **50**, 3650 (1994), doi:[10.1103/PhysRevA.50.3650](https://doi.org/10.1103/PhysRevA.50.3650).
- 563 [43] I. Medina, F. J. García-Vidal, A. I. Fernández-Domínguez and J. Feist, *Few-mode field*
564 *quantization of arbitrary electromagnetic spectral densities*, Phys. Rev. Lett. **126**, 093601
565 (2021), doi:[10.1103/PhysRevLett.126.093601](https://doi.org/10.1103/PhysRevLett.126.093601).
- 566 [44] D. Tamascelli, A. Smirne, S. F. Huelga and M. B. Plenio, *Nonperturbative treatment of*
567 *non-markovian dynamics of open quantum systems*, Phys. Rev. Lett. **120**, 030402 (2018),
568 doi:[10.1103/PhysRevLett.120.030402](https://doi.org/10.1103/PhysRevLett.120.030402).